Available online at www.sciencedirect.com

ScienceDirect

Energy Procedia 80 (2015) 302 – 311

Energy Procedia

EERA DeepWind'2015, 12th Deep Sea Offshore Wind R&D Conference

Investigation of the impact of wakes and stratification on the performance of an onshore wind farm

Mandar Tabib[a,*], Adil Rasheed[a], Trond Kvamsdal[a,b]

[a]*Applied Mathematics, SINTEF ICT, Strindveien 4, Trondheim 7035, Norway*
[b]*Mathematical Sciences, NTNU, Alfred Getz vei 1, Trondheim 7491, Norway*

Abstract

This work investigates the effects of wakes and stratification on the performance of turbines operating in the Bessaker wind farm. The wind farm is located in a highly complex terrain. Most dominant wind directions recorded close to the site are westerly and south easterly and the average wind speed is recorded in the range of $10-15m/s$ implying that the turbines are rarely idle. However, the power production data of individual turbines revealed that a few turbines were almost always under-performing. This matter was earlier investigated using a multi-scale model ([1]) involving meso-scale weather forecasting model providing input to a nested micro-scale CFD code. This previous study hinted at strong thermal stratification as the culprit which causes a channeling effect thus reducing the wind potential available uphill. However, wake effects were completely ignored in those studies. The current work includes an actuator line (AL) model to enable simulation of wake effects along with stratification and terrain effects on turbine behavior. As a result, the model is able to capture the delay in wake recovery during stable stratified conditions and the resultant turbine-turbine interactions leads to the reduced power production at wind-farm. The inclusion of wake effects showed that the current inter-turbine distance of 4 rotor turbine diameter at some locations is not good for wind-farm operation. This effect was not captured by the earlier multi-scale model which lacked the AL model. Further, the work shows some differences in results arising out of two models (current and previous multi-scale model) related to channeling effect. This difference is attributed to difference in thermal stratification level (Froude number) as the current model uses standard atmospheric inlet profiles/initial profiles, while the multi-scale model used inputs from the higher meso-scale weather forecasting model. The overall work indicates the importance of including wake and stratification effects and the importance of downscaling (using inputs from weather-forecasting models) in improving predictions. According to the authors this is the first work of its kind which accounts for stratification, complex terrain and wakes in a single simulation.

Peer-review under responsibility of SINTEF Energi AS

Keywords: Wind Farm, Stratification, Terrain induced turbulence, Wake effects, Actuator line, CFD

1. Introduction

The wind energy has immense potential to contribute towards global energy demand and it will increase further provided the cost of wind-energy (CoE) remains competitive. Over the past decade, the CoE has reduced owing

* Corresponding author. Tel.: +47-92011677
E-mail address: mandar.tabib@sintef.no, adil.rasheed@sintef.no, trond.kvamsdal@sintef.no

Peer-review under responsibility of SINTEF Energi AS
doi:10.1016/j.egypro.2015.11.434

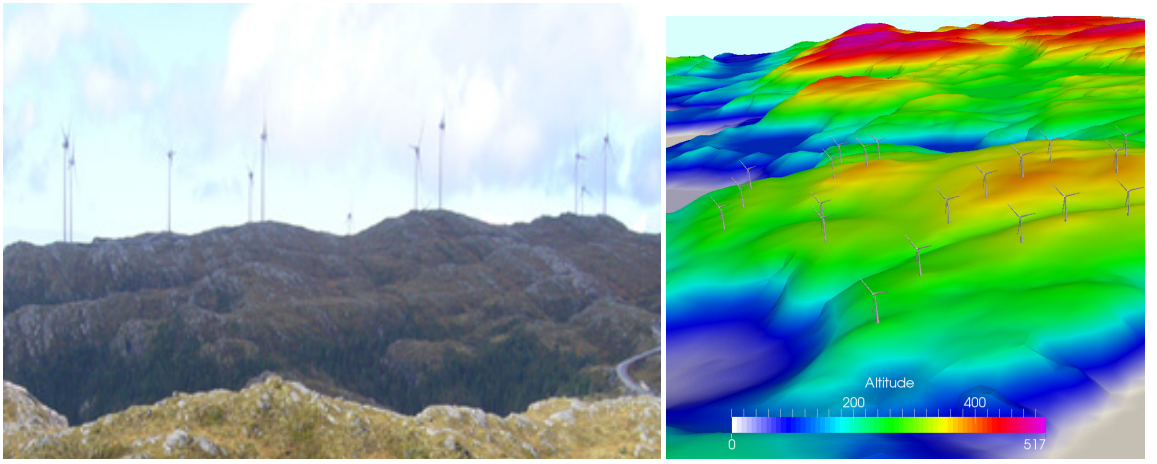

(a) Bessaker wind farm (b) Digital model (Altitude in m)

Fig. 1. Bessaker wind farm

to significant improvements in turbine technologies (involving longer and lighter blades, efficient blade designs and effective operational control practices). Research continues to be devoted to make wind energy more affordable, which will boost the wind energy contribution and help to create a cleaner and greener environment. In this direction, an accurate estimate of wind resource will help to determine the expected power production and associated cost at a given site. Wind resource within a particular farm-site is influenced by surrounding terrain conditions, atmospheric stratification (which changes during the 24 hrs. day) and wake effects (wherein upstream turbine generated wake influences downstream turbines)[2]-[6]. Most of the numerical wind models used to predict wind conditions/power production over-simplify the actual physics for sake of faster computational time, in at least one of these three ways: by (a) not accounting for a complex terrain geometry and simplifying its effect by using a roughness factor with a flat terrain (b) assuming neutral atmospheric conditions and ignoring stratified conditions and accompanying buoyancy effects (c) using simplified wake models.

These simplified assumptions may give faster results but at the cost of accuracy. In this work, we have developed an advanced numerical model that can account for effects of highly complex terrain, atmospheric stratification and wake effects in a multi-turbine wind farm. The objectives of this work are two folds: firstly to test the predictive ability of this advanced numerical model, and influence of different components (e.g. with/without atmospheric stratification) on wind dynamics in a wind farm and secondly to apply this model on a realistic industrial wind farm for troubleshooting/designing it and encourage usage of advanced models with more physics for industrial wind farms.

This model has been applied on a realistic industrial wind-farm called Bessaker Wind Farm, which is operated by TrønderEnergie AS. The verification of results obtained by the model has been done with the observed power production trends at the Bessaker Wind Farm. The technical aspects about the Bessaker Wind Farm is given in the next section, followed by details of this advanced model, solution methodology, results and discussion and conclusion.

2. Bessaker wind farm and problem statement

Bessaker wind farm (Figure 1) is operated by TrønderEnergie AS, one of the largest energy provider in Norway. The farm is a located in a complex terrain in mid-Norway region near Trondheim. The hilly terrain rises from sea level to a maximum altitude of $500m$. The onshore wind farm established on this complex terrain has 25 turbines, which are located at different altitudes in the terrain. The base of lowest turbine is located at $240m$ above sea level and the highest turbine is located at about $385m$ above sea level. Rest of the turbines are within the altitude range. All the 3 bladed turbine used in the wind farm have a rated power of $2.3MW$, a rotor diameter of $71m$ and a hub height of $64m$ with cut-off speed at about $28m/s$ wind. Generally, most dominant wind directions recorded at this site at $35m$ above the ground is westerly and south easterly and the average wind speed is recorded in the range of $10-15m/s$ implying

that the turbines are rarely idle. However, a closer look at the power production of individual turbines reveals that a few turbines are almost always underperforming and overall power production is low. Computational Fluid Dynamics (CFD) was used to understand why this could be occurring. This wind farm was taken to test the model.

3. Model details

A transient 3D CFD model is developed which can account for thermal stratification and wake effects. The CFD model computes the flow field (velocity, pressure, temperature) and turbulence field in the wind farm by solving an Reynolds averaged Navier Stokes (RANS) equation. RANS equation set consists of averaged mass continuity equation (Equation 1), averaged momentum transport equation (Equation 2) , averaged thermal transport equation (Equation 3), transport equations for turbulent kinetic energy (Equation 5) and turbulent kinetic energy dissipation rate (Equation 6). The thermal stratification effects are included by incorporating the buoyancy induced turbulence (Equation 7) and assuming Boussinesq approximation for density (so, density variations are only considered in the gravity term). Currently, the model does not account for moisture and the associated condensation when air parcels are lifted, which can affect the stability of the air. The turbines and subsequent wake effects are modeled using actuator line (AL) approach. The AL model (Equation 8, 9, 10) uses the velocity field ($\mathbf{u}$) as input from RANS CFD model and outputs body force, which are used as the sink term in the momentum equation. The AL approach resolves each blade of the turbine as a rotating line (made of N actuator segments), over which the forces are computed. The force at each segment comprises of lift force (L in equation 8) and drag forces (D in equation 9), which are computed from the local relative velocity (V_{rel}, local twist angle, blade chord (c), local actuator width (w) and local angle of attack (α) at a given actuator segment. The local angle of attack is computed from the tangential and normal component of relative velocity at the segment. The lift coefficient C_l and drag coefficient C_d at each segment (in Equation 8, 9) are a function of local angle of attack, and this dependency is provided as an input (blade airfoil data) to the AL model. The force at an actuator segment is a point force and it is translated on to the fluid domain as a volumetric body force using Gaussian projection (Equation 10). The regularization parameter (ε) in Equation 10 represents the width of the Gaussian and determines the concentration of the force. Larger the parameter, more smoothed out the force is on flow field. The negative sign in Equation 10 accounts for the fact that the force exerted by turbine on the flow field is equal and opposite to the force experienced by it due to the flow. At the location (x, y, z) of the fluid domain, the overall body force is summation of force over all N actuator segments of the turbine, where (x_j, y_j, z_j) is the location of the j^{th} segment and r_j is the distance between segment j and the fluid domain location. The equations solved and their notations are mentioned below :

$$\nabla \cdot (\rho \mathbf{u}) = 0 \tag{1}$$

$$\frac{D\mathbf{u}}{Dt} = -\nabla\left(\frac{p}{\rho}\right) + \mathbf{g}\frac{\theta}{\theta_0} + \frac{1}{\rho}\nabla \cdot \mathbf{R} + \mathbf{f} \tag{2}$$

$$\frac{D\theta}{Dt} = \nabla \cdot (\gamma_T \nabla\theta) + q \tag{3}$$

where, operator $\frac{D}{Dt}$ refers to total derivative, operator ∇ refers to computing gradient, operator $\nabla\cdot$ refers to computing divergence, t is time, ρ is density,p is pressure, θ is potential temperature,θ_0 is reference potential temperature, $\mathbf{f}$ refers to external forces arising from actuator line model, q refers to heat source/sink, $\mathbf{R}$ is referred to turbulent stresses and arises owing to averaging procedure. Components of $\mathbf{R}$ can be computed as $R_{ij} = \nu_T\left(\frac{\partial u_i}{\partial x_j} + \frac{\partial u_j}{\partial x_i}\right) - \frac{2}{3}k\delta_{ij}$, where subscripts i, j refers to components of vector, k is turbulent kinetic energy and ν_T ($=\mu_t/\rho$) is turbulent diffusivity. The turbulent eddy viscosity (μ_t, equation 4) is formulated in terms of turbulent kinetic energy (k) (equation 5) and turbulent kinetic energy dissipation rate(ϵ) (equation 6).

$$\mu_t = C_\mu \frac{k^2}{\epsilon} \tag{4}$$

where $C_\mu = 0.09$ is a constant.

$$\frac{Dk}{Dt} = \nabla \cdot (\nu_T \nabla k) + P_k + G_\theta - \epsilon \tag{5}$$

where P_k is production of turbulent kinetic energy due to shear and G_θ is production of turbulent kinetic energy due to buoyancy induced turbulence and are calculated using equation (7).

$$\frac{D\epsilon}{Dt} = \nabla \cdot \left(\frac{\nu_T}{\sigma_e} \nabla \epsilon \right) + (C_1 P_k + C_3 G_\theta) \frac{\epsilon}{k} - C_2 \frac{\epsilon^2}{k} \tag{6}$$

where σ_e =1 and σ_e =1.3 are turbulent prandtl numbers, and C_1=1.44 ,C_2=1.92,C_3 = 1.44 are constants.

$$P_k = \nu_T \left(\frac{\partial u_i}{\partial x_j} + \frac{\partial u_j}{\partial x_i} \right) \frac{\partial u_i}{\partial x_j}, \quad G_\theta = -\frac{g}{\theta} \frac{\nu_T}{\sigma_T} \frac{\partial \theta}{\partial z} \tag{7}$$

$$L = \frac{1}{2} C_l(\alpha) \rho V_{rel}^2 cw \tag{8}$$

$$D = \frac{1}{2} C_d(\alpha) \rho V_{rel}^2 cw \tag{9}$$

$$F_i^T(x, y, z) = -\sum_{j=1}^{N} f_i^T(x_j, y_j, z_j, t) \frac{1}{\varepsilon^3 \pi^{3/2}} exp\left[-\frac{r_j^2}{\varepsilon} \right] \tag{10}$$

4. Solution methodology

4.1. Solver details

The solver has been created in OpenFOAM-2.3.0 (OF). An elliptic equation for the modified pressure is created to ensure continuity by combining continuity equation with divergence of momentum equation. This elliptic equation along with the momentum equation, potential temperature equation and turbulence equation are solved in a segregated manner using the PISO-SIMPLE algorithm (PIMPLE algorithm). The PIMPLE algorithm ensures use of a higher time-step for transient simulations. The OF uses a finite volume discretization technique, wherein all the equations are integrated over control volumes (CV) using Green Gauss divergence theorem. The gauss divergence theorem converts the ”volume integral of divergence of a variable” into ”surface integral of the variable over faces comprising the CV”. Thus, the divergence term defining the convection terms can simply be computed using the face values of variable in the CV. The face values of variable are obtained from its neighboring cell centered values by using convective scheme. In this work, all the equations (except k and turbulence equations) uses second order linear discretization scheme, while the turbulent equations use upwind convection schemes. Similarly, the diffusion term involving laplacian operator (the divergence of the gradient) is simplified to computing the gradient of the variable at the face. The gradient term can be split into contribution from the orthogonal part and the non-orthogonal part. A full non-orthogonal correction is implemented for all equations as solver stability won't be a problem owing to good mesh used. The mesh details, CFD domain set-up, boundary and initial conditions are defined below.

4.2. Simulation set-up

The Bessaker wind-farm CFD set-up involves a domain size of $6.8km \times 4.5km \times 1.5km$ (Figure 2). This domain size ensures that entire wind-farm area is considered and the location of domain boundary will not affect the flow profile within wind farm. A westerly wind-flow is considered for this simulation as this is one of the dominant wind direction at the site. The terrain geometry is included in the domain as an STL file and the domain and mesh is built using it. The mesh size for this domain is about 13 million cells. The grid is finer in the wind-farm region and near the terrain, where the velocity gradient is high and effect of wake has to be captured. The finest grid size in wind-farm region is $6m$ in every direction and the coarsest grid size in every direction is 50m (in regions away from wind farm and terrain). This ensures that there are at least 10 numerical cells within the turbine area, as the rotor blade is of $60m$ diameter. The time step used for simulation has been more stringent than normal CFL criteria of 1. The time-step was selected based on the tip speed and grid cell size in the AL domain. The time-step was such that the blade (rotating line) does not move more than one grid cell within a time-step. To achieve this, a time step of $0.015s$ was used which

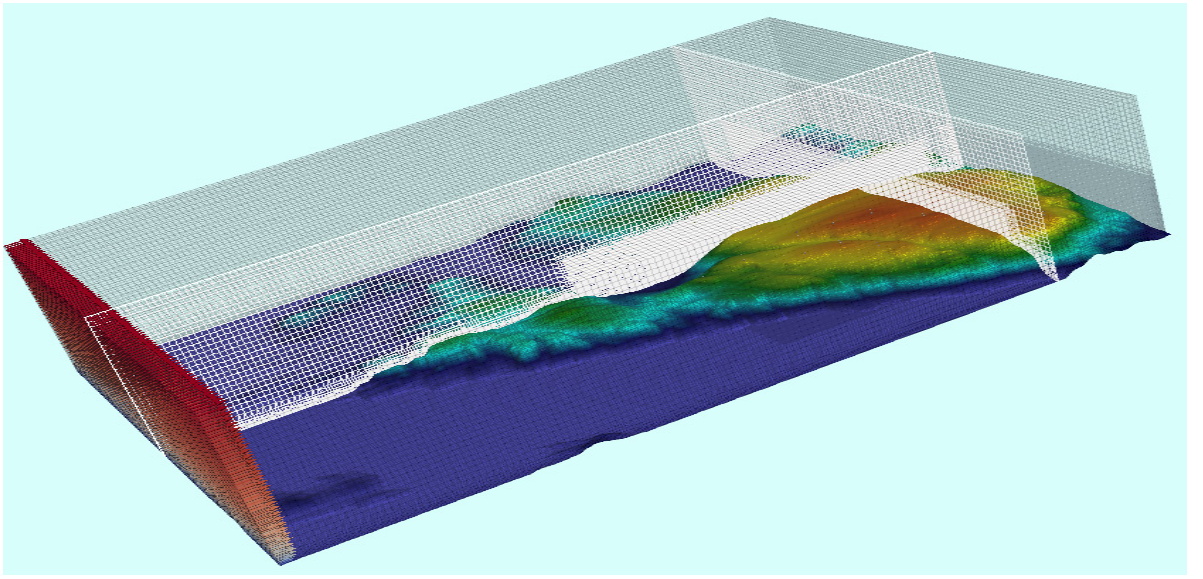

Fig. 2. CFD domain enclosing the terrain with 13 million cells. Two perpendicular slides shows the internal mesh. Westerly wind flows from inlet at left and the outlet on right.Top and side walls are slip boundary.

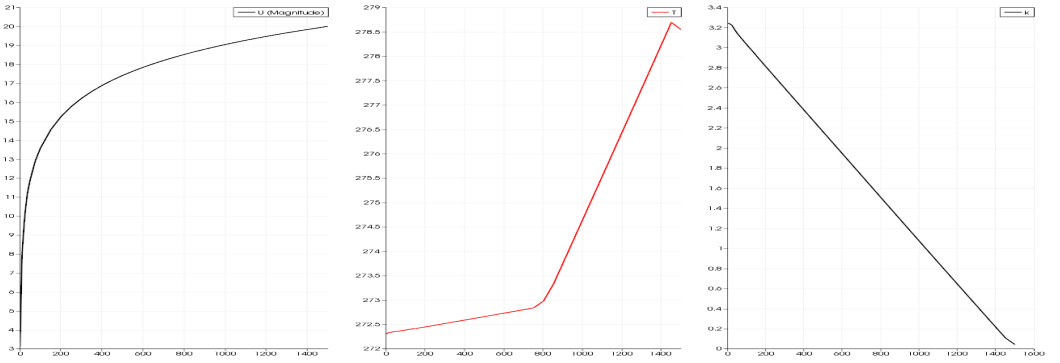

(a) Velocity profile (in m/s) (b) Potential temperature (in °K) (c) Turbulent kinetic energy (in m^2/s^2)

Fig. 3. Inlet profiles for Velocity (leftmost), Potential temperature (middle) and turbulent kinetic energy (right) as function of vertical distance from the ground (X axis).

gave a CFL of 0.15. An Euler discretization scheme is chosen for temporal discretization. The solver was run on 216 parallel processors The simulation has been carried out for two cases: (a). Neutral Atmospheric condition (b). Stable thermal atmospheric stratification condition.

Figure 3 shows the inlet boundary conditions (velocity condition, potential temperature and turbulent quantities) specified for these two as per the atmospheric boundary layer profile represented by Equations 11, 12 and 13. An inlet potential temperature profile is defined for the stable stratification condition, while no potential temperature equation is required to be solved for the neutral boundary condition. The side and top boundary conditions of the domain are slip walls. The outlet has fixed pressure boundary conditions. The bottom terrain geometry is no-slip boundary condition, and for the stable atmospheric condition, a fixed temperature (variable hear flux) is defined for the bottom terrain boundary.

$$u_{inlet}(z) = \frac{u_*}{\kappa}(ln\frac{z}{z_0}) \tag{11}$$

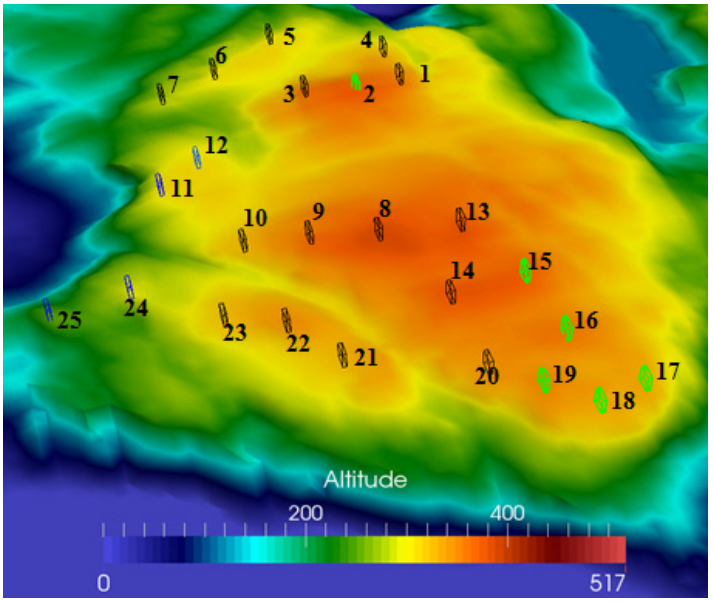

Fig. 4. Location and performance of 25 turbines (altitude in m). Green colored turbines producing highest power, blue colored turbine producing lowest power and the rest black colored are in between.

where u_{inlet} is velocity, z is distance from the ground, $\kappa = 0.4$ is constant, u_* is friction velocity, z_0 is local surface roughness height that represents the height above ground where the wind speed goes to zero. Its value is taken as 0.3 m considering the terrain at the inlet region.

$$k_{inlet}(z) = C_\mu^{-1/2} u_*^2 \left(1 - \frac{z}{D}\right) \tag{12}$$

$$\epsilon_{inlet}(z) = \frac{C_\mu^{0.75} k(z)^{1.5}}{\ell}; \ell = \frac{\kappa z}{(1 + 4z/D)} \tag{13}$$

Figure 4 shows the location of the 25 turbines on the terrain. The effect of turbines is accounted using the Actuator line method as explained in section 4. For AL approach, about 40 actuator segments were used in the simulation. The regularization parameter (ε) was chosen to be about two times the cube root of grid volume size in that region. This was selected so as to ensure that the force is not overly concentrated to cause numerical oscillations/solver instability, and neither does the force becomes too smoothed so as to cause no resistance to the wind flowing through the turbine. The next section discusses the results obtained.

5. Results

5.1. Neutral condition

The simulations were conducted for westerly wind direction involving neutral atmospheric condition (using inlet profiles shown in Figure 3a-b)). The inclusion of complex terrain in the simulation helps to capture phenomena related to wind acceleration/deceleration as a result of altitude changes. The wind speeds-up while ascending as streamlines converge and wind decelerates as it descends down a hill. This effect along with flow separations (if any) will not be captured when using a flat-terrain geometry with roughness. Hence, the turbines shown in green color in Figure 4 (Turbine number 2, 15, 16, 17, 18, 19) are producing higher power output, while the turbines shown in blue color in Figure 4 (Turbine number 11, 12 , 24 ,25) are producing the least power output. The streamline in Figure 5 shows the higher velocity wind region (wind speed above $15m/s$, up-to $20 - 22m/s$) at location of green colored turbines.

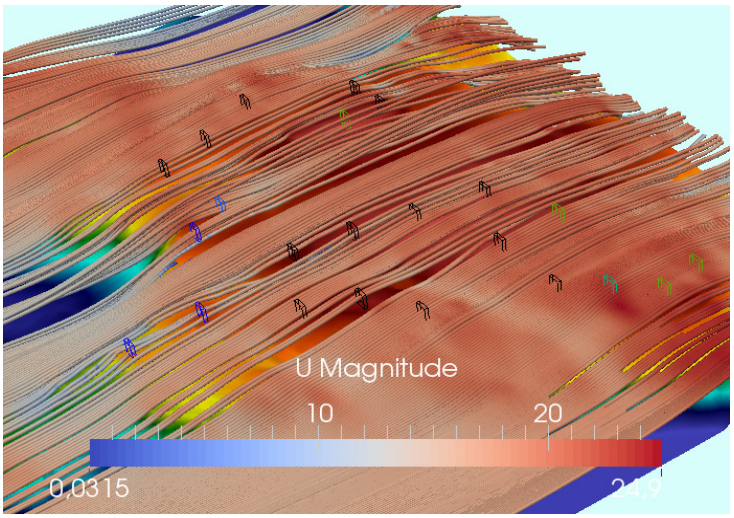

Fig. 5. Streamlines showing the regions of higher wind velocity (in m/s) near green colored turbines (Turbine 2, 15-19) and lower wind velocity (in m/s) at regions of blue colored turbines (Turbine 11,12,24,25).

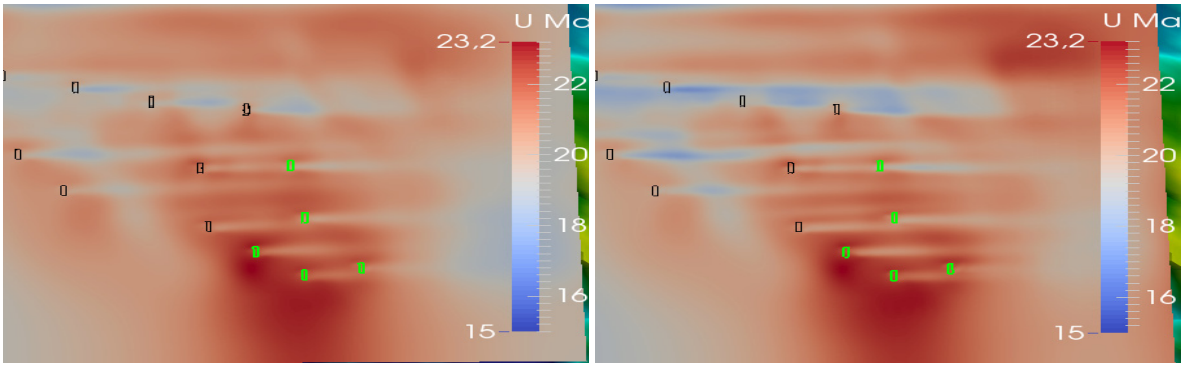

(a) Neutral condition: Wake Velocity deficit (unit in m/s)

(b) Stable stratified: Wake Velocity deficit (unit in m/s)

Fig. 6. Contour of velocity magnitude on horizontal plane above the wind farm for neutral and stable condition. Wake velocity deficit is seen behind turbine locations. Velocity deficit is more pronounced under stable conditions.

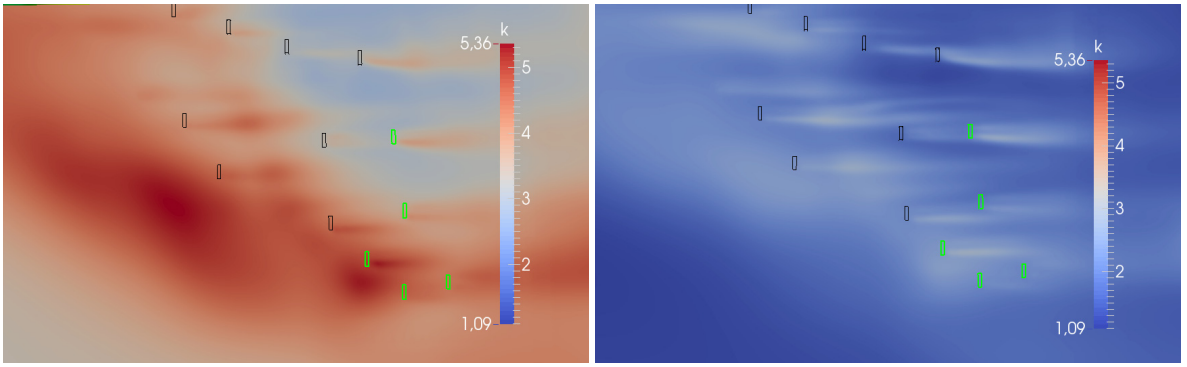

(a) Neutral: Turbulent kinetic energy (in m^2/s^2)

(b) Stable stratified: Turbulent kinetic energy deficit (in m^2/s^2)

Fig. 7. Turbulent kinetic energy profiles for neutral and stable condition. Higher atmospheric turbulence seen in neutral case, while Stable stratification has lower turbulence levels.

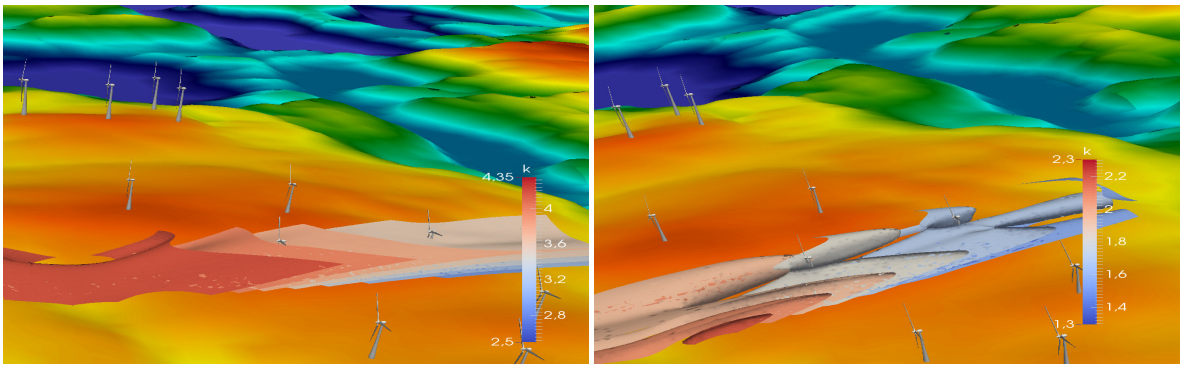

(a) Neutral condition: Isocontours of k (in m^2/s^2). High turbulence seen but no wake like structure between turbine 14-15.

(b) Stable condition: Isocontours of k (in m^2/s^2). Lower turbulence but wake structures exist and extends from turbine 14 to 15

Fig. 8. Isocontours of k between turbine 14-15 for neutral and stable conditions.

These turbines are located at higher altitude and experience good wind speeds. While, the turbines in blue are at lower altitude and experience comparatively lower wind speed between $5 - 15m/s$ and hence, provides lower power output. These results are on contrast to that observed using our earlier multi-scale work as multi-scale work includes different wind directions (mainly, south easterly which enhance power production of Turbine 24-25-11-12) and also, the extent of stratification is different which causes channeling (as discussed below) . The wake velocity deficit regions can also be seen and this is discussed later in section 5.3.

5.2. Stably stratified condition

Further, it is interesting to see the effect of thermal stratification in this work. Thermal stratification generally causes either channeling (thus reducing wind potential upstream) or delays wake decay, both of which results in lower power production. However, for the present simulation conditions, the power produced declined only by $1 - 2\%$ as compared to the neutral case. The reduction in power produced is less than that predicted by earlier multi-scale model because predominant channeling effect is not observed in this simulation result. For the present condition, the potential temperature gradient over the height of the hill is low (see low slope of gradient at lower part of altitude in Figure 3) and wind speed is high, as a result the restoring buoyant force as wind rises on the hill is lower than the kinetic energy of the wind (the Froude number is much higher than one, it is about 5, $Fr = U/(H * N)$). Hence, the flow does not face major resistance while ascending the hill and goes over the hill instead of sideways flow, thus channeling is not observed. Huge channeling was seen in the earlier multi-scale simulation because the input on extent of thermal stratification provided by meso-scale weather forecasting model was more than the standard profile used in this work. Thus, we see how the results can be vary due to change in atmospheric conditions. In current case, the slightly lower production in stratification condition can be attributed to the enhanced effect of wakes, as discussed below.

5.3. Effect of Wakes in Stable Vs Neutral condition

The computed power from simulation shows that few turbines produce less power in stratified conditions as compared to neutral conditions (like, turbine number 2 and 15). This is because turbines 2 and 5 are affected by the wakes of upstream turbines (turbine 3 and 14 respectively), as their rotors lie on same altitude owing to flattish terrain at the top of hill. Figure 6 compares the wake velocity deficit for neutral and stratified flows. The velocity deficit region behind turbines for stratified flow is seen to be more pronounced and extended, for example compare wake behind turbine 8,9,13, 14 and 15. Turbine 14 wake reaches out farther till turbine 15 in stratified as compared to neutral. The decay of wake is slow in stable stratified conditions owing to lower momentum transfer and lower mixing at the reduced atmospheric turbulence (buoyancy suppresses vertical fluctuations in stable case). Hence, the wake extends well beyond the current inter-turbine distance (which is 4 times the rotor diameter). Figure 7(a) shows a higher atmospheric turbulence level for neutral condition than for the stable stratified case (Figure 7(b)). The wakes in Figure 7(b)

behind the rotor region extends longer than wakes in Figure 7(a). Same can be observed in Figure 8, which shows the turbulent wake structure through iso-contour of turbulent kinetic energy. Figure 8a shows higher values of turbulent kinetic energy but no definite wake structure exist in neutral case. Figure 8(b) for stable stratified conditions shows low turbulence levels but a definite wake structure that extends from turbine 14-15. Generally, the normal practice is to place turbines at a distance of 10 times rotor diameter, but this is not the case here. Few of the turbines at the top of the hill are located at 4-5 times rotor diameter distance. Hence, under stratified conditions, turbine-turbine interactions exist owing to longer wakes as seen in Figure 6-8. The reduced velocity experienced by the downstream turbines owing to wake effect leads to lower power production. Hence, the power production is 2% lower for stable stratified case than the neutral case. The next section presents the conclusion from this work.

6. Conclusion and future work

A model has been developed that simulates wake effects along with thermal stratification and terrain effects to capture power production in multi-turbine wind farm. The inclusion of terrain geometry leads to higher wind speed-up and more power output from turbines at higher altitudes in neutral conditions. The model has also been able to capture the effect of stratification on wake evolution and give insights about reduced power scenario in stratified condition (as compared to neutral conditions). The numerical model predicts lower turbulence in stable stratified conditions which delays wake recovery and causes lower power production. In normal practice, wind farms have the turbines at a distance of 10 times the rotor diameter whereas at Bessaker for some of the turbines it is only 4-5 times rotor diameter and this has an impact on the turbine-turbine interactions (which has been captured by the current model). This effect was not captured by the earlier multi-scale model ([1]) as it lacked the AL model and could not simulate wake deficit effects. Interestingly, the results of current model vary from the earlier multi-scale model in terms of amount of channeling seen during stratification. This could be owing to different thermal stratification used in the present study, which results in a higher Froude number signifying lower restoring buoyant force on the ascending wind. The multi-scale model provides more accurate thermal boundary conditions as it uses the meso-scale weather forecasting model for input conditions rather than using standard atmospheric inlet boundary profiles/initial profiles (which have been used in current work). Thus, current work indicates the importance of including wake and stratification effects and importance of downscaling (using inputs from weather-forecasting models) in improving predictions. Hence, future work may involve developing this model further by nesting the meso-scale weather forecasting model with this model , and/or incorporating moisture effects, and/or improving understanding of wake-plume interactions by incorporating LES turbulence model ([9]) with thermal stratification. These model additions will be validated with experimental data. It is also worth stating here that the input parameters in AL model related to blade like lift & drag coefficients do not correspond to the actual turbine blades operational in the wind farm. However, with generalized mesh generators like the one presented in [7] and two dimensional simulation tools based on isogeometric analysis ([8]) it would be possible in the very near future to generate the input parameters for specific turbine blades in use.

Acknowledgements

The authors would like to acknowledge the financial support from the Norwegian Research Council and the industrial partners of the FSI-WT (http://www.fsi-wt.no) project (Kjeller Vindteknikk, Statoil, Trønder Energi AS and WindSim). We are also thankful to Ingrid Vik and Magne Røen from TrønderEnergie for providing information on the locations of turbines in the Bessaker wind farm and the information on turbines.

References

[1] Rasheed A, Sørli K, Holdahl R, Kvamsdal T, A Multiscale Approach to Micrositing of Wind Turbines, Energy Procedia 2012;14:1458-1463.
[2] Churchfield MJ, Lee S, Michalakes J, Moriarty PJ, A numerical study of the effects of atmospheric and wake turbulence on wind turbine dynamics, Journal of Turbulence 2012;N14.
[3] Churchfield MJ, Lee S, Moriarty PJ, Martnez LA, Leonardi S, Vijayakumar G, Brasseur JG, A large-eddy simulation of wind-plant aerodynamics, 50th AIAA Aerospace Sciences Meeting Including the New Horizons Forum and Aerospace Exposition, 2012
[4] Keck RE, Mar MDe, Churchfield MJ, Lee S, Larsen G, Madsen HA, On Atmospheric Stability in the Dynamic Wake Meandering Model, Wind Energy, 2014;17:1689-1710.

[5] Lee S, Churchfield MJ, Moriarty PJ, Jonkman J, Michalakes J, A Numerical Study of Atmospheric and Wake Turbulence Impacts on Wind Turbine Fatigue Loadings, Journal of Solar Energy Engineering, 2013;135(3):31001-10
[6] Akbar M, Port-Agel F, The Effect of Free-Atmosphere Stratification on Boundary-Layer Flow and Power Output from Very Large Wind Farms, Energies 2013;6:2338-2361
[7] Fonn E, Rasheed A, Kvarving A, Kvamsdal T, Tabib M, Opstal T, Spline based mesh generator for high fidelity simulation of flow around turbine blades. In EERA DeepWind 2015, 12th Deep Sea Offshore Wind R&D Conference. 2015
[8] Nordanger K, Holdahl R, Kvarving A, Rasheed A, Kvamsdal T, Implementation and comparison of three isogeometric Navier-Stokes solvers applied to simulation of flow past a fixed 2D NACA0012 airfoil at high Reynolds number. Computer Methods in Applied Mechanics and Engineering 2015;284(0):664-688.
[9] Tabib M., Rasheed A, Kvamsdal T, LES and RANS simulation of onshore Bessaker Wind farm: analyzing terrain and wake effects on wind farm performance . Journal of Physics: Conference Series 2015; 625: 012032.